Subduction of the Chile Ridge: Upper Mantle Structure and Flow

R. M. Russo[1], John C. VanDecar[2], Diana Comte[3], Victor I. Mocanu[4], Alejandro Gallego[1], and Ruth E. Murdie[5*]

[1]*Department of Geological Sciences, University of Florida*

[2]*Department of Terrestrial Magnetism, Carnegie Inst. of Washington*

[3]*Departamento de Geofisica, Universidad de Chile, Santiago*

[4]*Department of Geophysics, University of Bucharest*

[5]*Comprehensive Test Ban Treaty Organization, Vienna*

* Now at: St. Ives Gold Mining Company, Kambalda, AUSTRALIA

SUPPLEMENTARY MATERIAL

TRAVEL TIME INVERSIONS

Arrival times for the *P* waves were determined via a multi-channel cross-correlation procedure that makes use of the duplicate information obtained by cross-correlating all possible pairs of waveforms (VanDecar and Crosson, 1990; VanDecar et al., 2003). This procedure produces both highly accurate delay times (~0.03 s) and useful standard error estimates. Each event was individually analyzed with various filter and cross-correlation settings to test for consistency and to ensure against cycle skipping and biases induced by waveform distortion. We parameterized variations in Earth structure beneath the stations with splines under tension constrained at a series of regular knots (Neele et al., 1993b; VanDecar et al., 2003), which allows both smooth slowness variations and maintains structure locally. Typical model knot spacing is ~33 km in the interior of the model (Supp. Fig. DR1), where we obtained the highest resolution. We restrict our interpretations to this interior region. Knots in the exterior region were included to mitigate against the mapping of unwarranted and spurious structure in outside regions into the model (Neele et al., 1993a,b; VanDecar et al., 2003).

We inverted simultaneously for slowness (1/velocity), earthquake locations, and station corrections. The station corrections are necessary to account for shallow crustal heterogeneity as well as differences in station elevation. We also used *P* wave core-phase arrivals (e.g., *PKP*) to include ray paths that impinge nearly vertically upon the network, enhancing lateral control on velocity anomalies. We searched for the simplest model necessary - that is, the model containing the least structure required to satisfy the observations to within their estimated standard errors (Constable et al., 1987; Neele et al., 1993b; VanDecar et al., 1995, 2003). We define “structure" by model derivatives, and seek to minimize spatial gradients and roughness equally, which is implemented numerically through first- and second-difference operators.

These large linear systems are inverted with a conjugate gradients procedure iterated to convergence (VanDecar and Snieder, 1994). We also iterated upon these inversions, systematically down-weighting equations associated with outlying residuals from the previous iteration (VanDecar et al., 2003). The effect of this is to produce a robust solution with L2 (least-squares) residual minimization within 1.5 residual standard deviations and, in the limit of many iterations, L1 (median) minimization for those equations associated with larger residuals (Huber, 1981). Experience has shown that even before robust down weighting, we can typically explain 95% of the root-mean-square data residual for *P* wave data (VanDecar et al., 1995; 2003). Finally, we perform three-dimensional ray tracing through the resulting model to find ray paths consistent with the three-dimensional model and repeat the linear inversion procedure.

We have done two types of resolution test, one intended to assess the degree to which we can image a gap in the lithosphere subducting beneath South America, and a second formulated to assess how well we can image isolated structures of either high or low velocity. Gaps in the slab at a suite of upper mantle depths are well recovered by these test inversions, but the strength of the slow velocity anomalies is typically underestimated and isolated anomalies can me smeared up to 100 km in depth. Therefore although we can be confident that the gaps in the subducted lithosphere exist, interpretations of the exact velocities in these gaps (and other secondary parameters potentially derived from these velocities, such as mantle temperature and viscosity) are not quantitatively reliable.

Simulated inversions for ‘checkerboard’ velocity anomalies show that resolution is best in the northern part of the study region, as expected, where logistics predicated siting of most of the CRSP stations, and that in the region of the observed low velocities we interpret as slab windows, we recover input structure reasonably well down to depths of around 400 km.

SEISMIC ANISOTROPY AND SHEAR WAVE SPLITTING

Laboratory experiments on natural and synthetic aggregates representative of dry upper mantle compositions indicate that when such rocks yield shear wave splitting, observed fast polarization directions parallel the (100) crystallographic axes of the aligned minerals (e.g., Hess, 1964; Carter et al., 1972; Kaminsky and Ribe, 2001), the type-A fabric of Jung et al. (2006). Compilations of natural upper mantle samples from locales around the globe indicate that the predominant form of upper mantle anisotropy follows this basic type-A fabric (Mainprice and Silver, 1993; Ben-Ismail and Mainprice, 1998). Jung et al. (2006) also note the existence of type-C and type-E fabrics which are petrographically distinct but which yield shear wave splitting with fast polarizations in the material flow direction similar to that produced by the A-type fabric (see their Fig. 12). Type-B fabrics which produce fast shear wave splitting polarizations parallel to olivine b-axes can be produced under high strain, or in the presence of significant water or melt fractions.

We used the method of Silver and Chan (1991) to determine splitting parameters; this involves minimizing the energy on the horizontal component corresponding to the minimum eigenvalue of the polarization matrix. Systematic checks of the measurements are done to ensure that the splitting parameters recovered are in fact the best pairs of fast polarization direction and delay time (Supp. Fig. DR3). Similar measurements were made for a suite of selected large-magnitude, deep, distant earthquakes which generated shear waves that traversed the Earth's core on their way to CRSP stations. Results with an interpretation of upper mantle flow directions in the vicinity of the two observed slab windows are shown in Supplementary Figure DR4.

We observe shear wave splitting that occurs in the upper mantle beneath CRSP stations, almost certainly entirely within the olivine stability fields (i.e., nominally 0-410 km depth). Given the clear and strong lateral heterogeneity in upper mantle structure in the vicinity of the two well-resolve

slab windows, it is to be expected that shear waves arriving from different backazimuths and distances would sample quite different upper mantle volumes – and hence upper mantle seismic anisotropy – on their upward paths to the CRSP recording stations. In order to gauge how different these paths are, and to visualize better the regions sampled by individual or suites of ray paths, we traced rays through a three-dimensional volume encompassing the study region (e.g., see Fig. 1 of the main text [GSA Today, v. 20, no. 9, p. 5]), utilizing velocities derived from the travel time inversions described in the text. An example of these ray paths is shown in Supplementary Figure DR5 for a subset of the events and a portion of the study region. Clearly, although the ray paths are typically steeply incident at the Earth's surface, they do diverge considerably at depth, and thus they sample quite distinct regions of the upper mantle beneath the CRSP network. Thus, upper mantle fabrics sampled by the arriving shear waves are likely to vary strongly, and observed shear wave splitting is also likely to vary as a consequence.

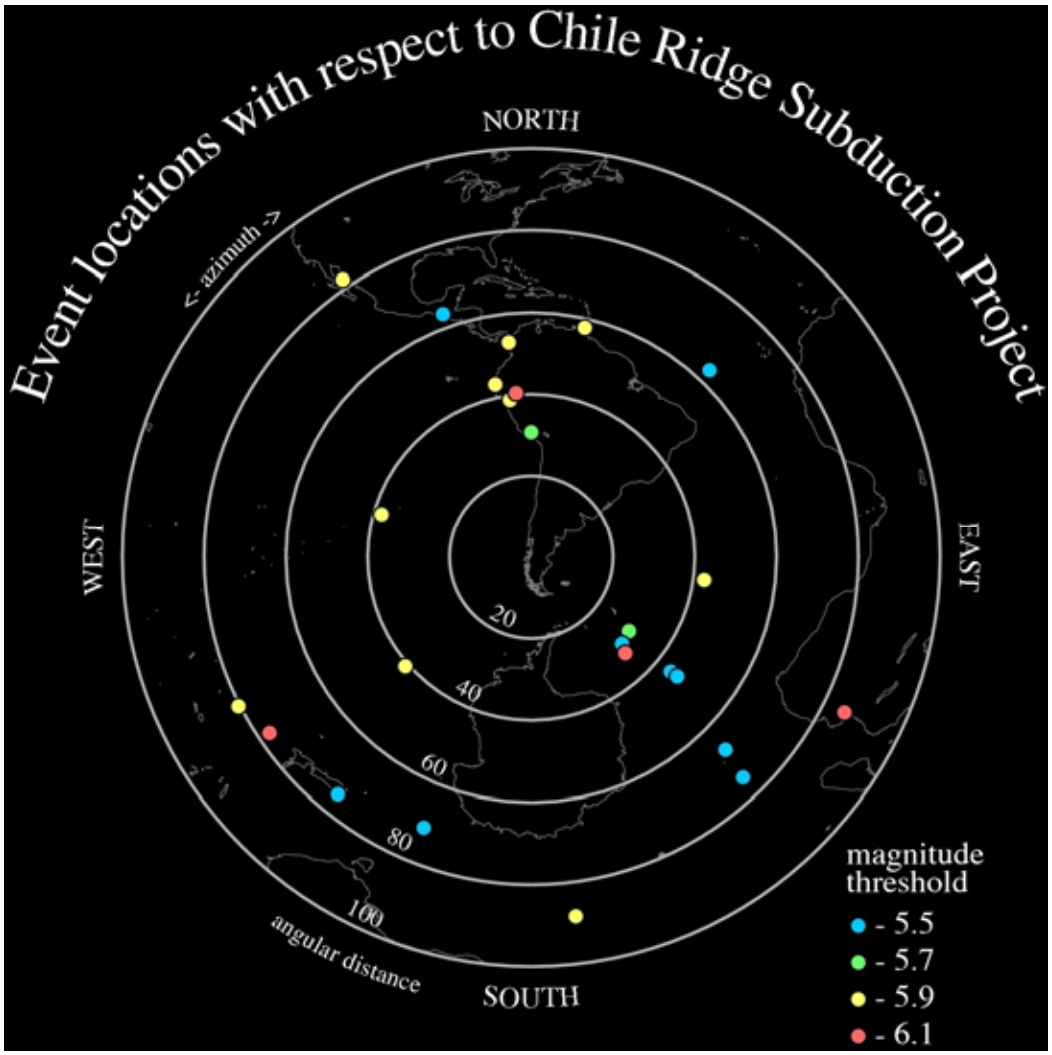

Supp. Figure DR1. *Events used for P wave travel time inversions to date (Dec. 2007). Plot center is the CRSP network, with distance (degrees of epicentral angle) between events and stations shown as concentric rings. Events with magnitudes between 5.5 and 6.1 (see key, lower right) were used.*

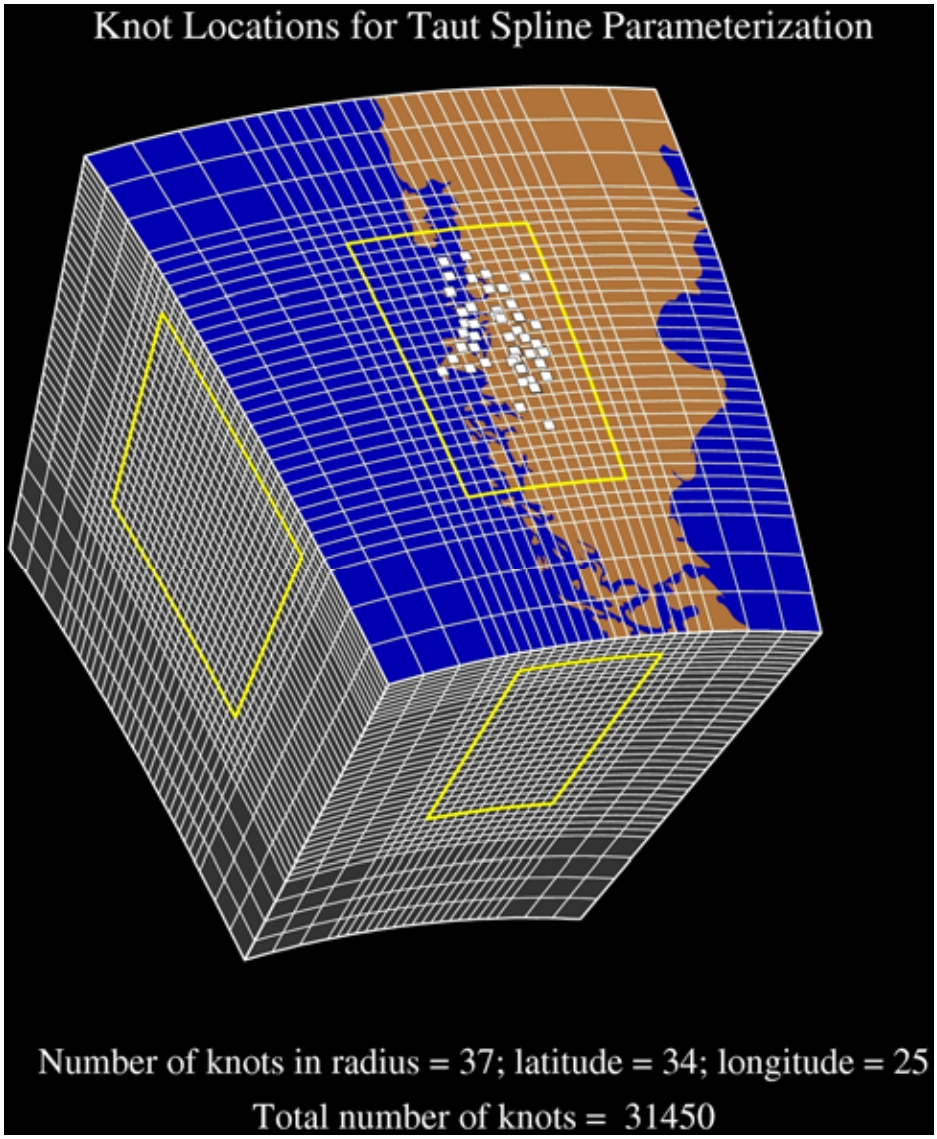

Supp. Figure DR2. *Grid of knots used for teleseismic travel time inversions. Yellow box delimits area of best resolution.*

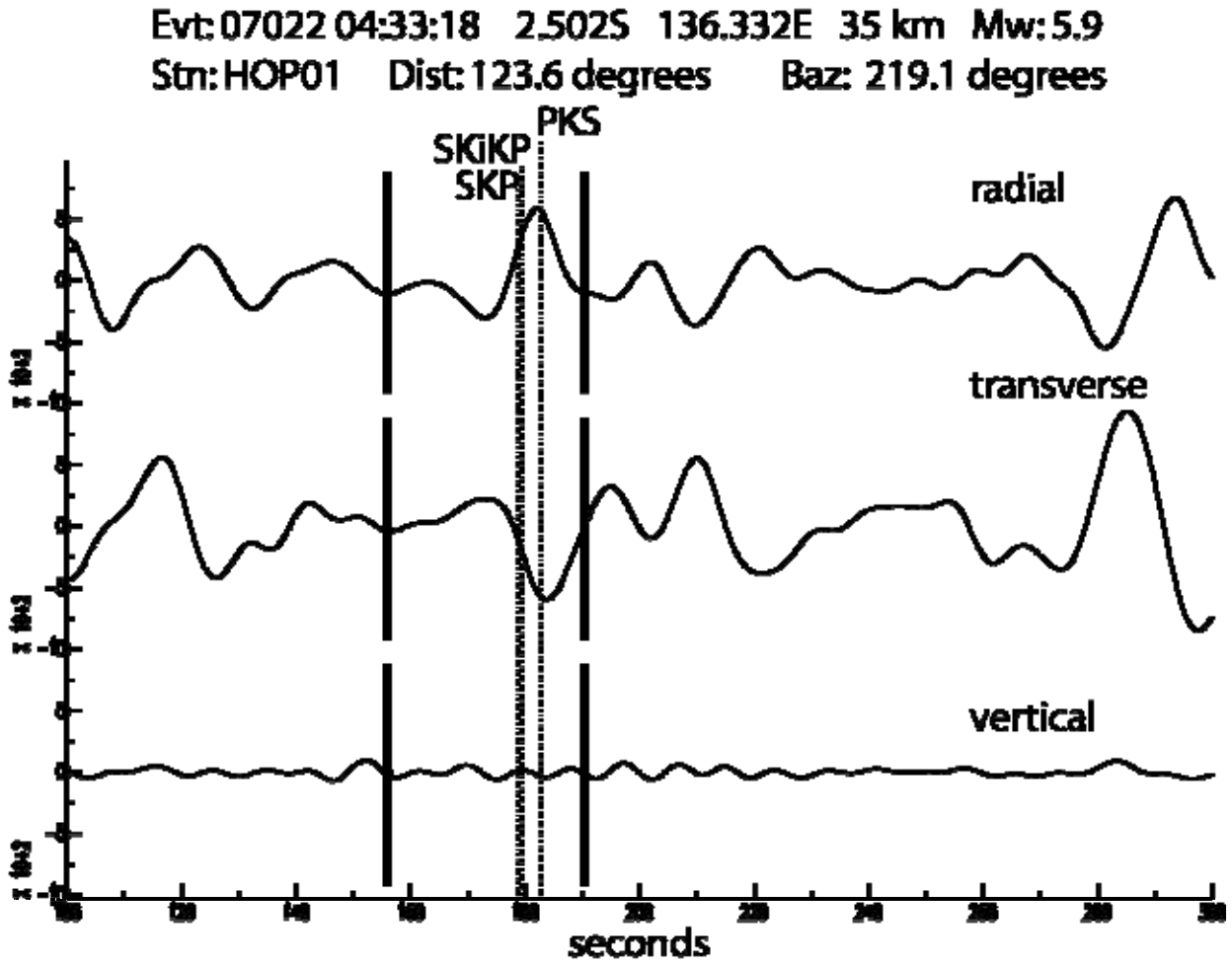

Supp. Figure DR3A. *Seismograms of SKS phase from an event on the SE Indian Ridge. Top two traces are rotated into the fast and slow frame, bottom two traces are showing the minimized energy on the linearized components after splitting correction. Lines labeled "A" and "F" mark the measurement window.*

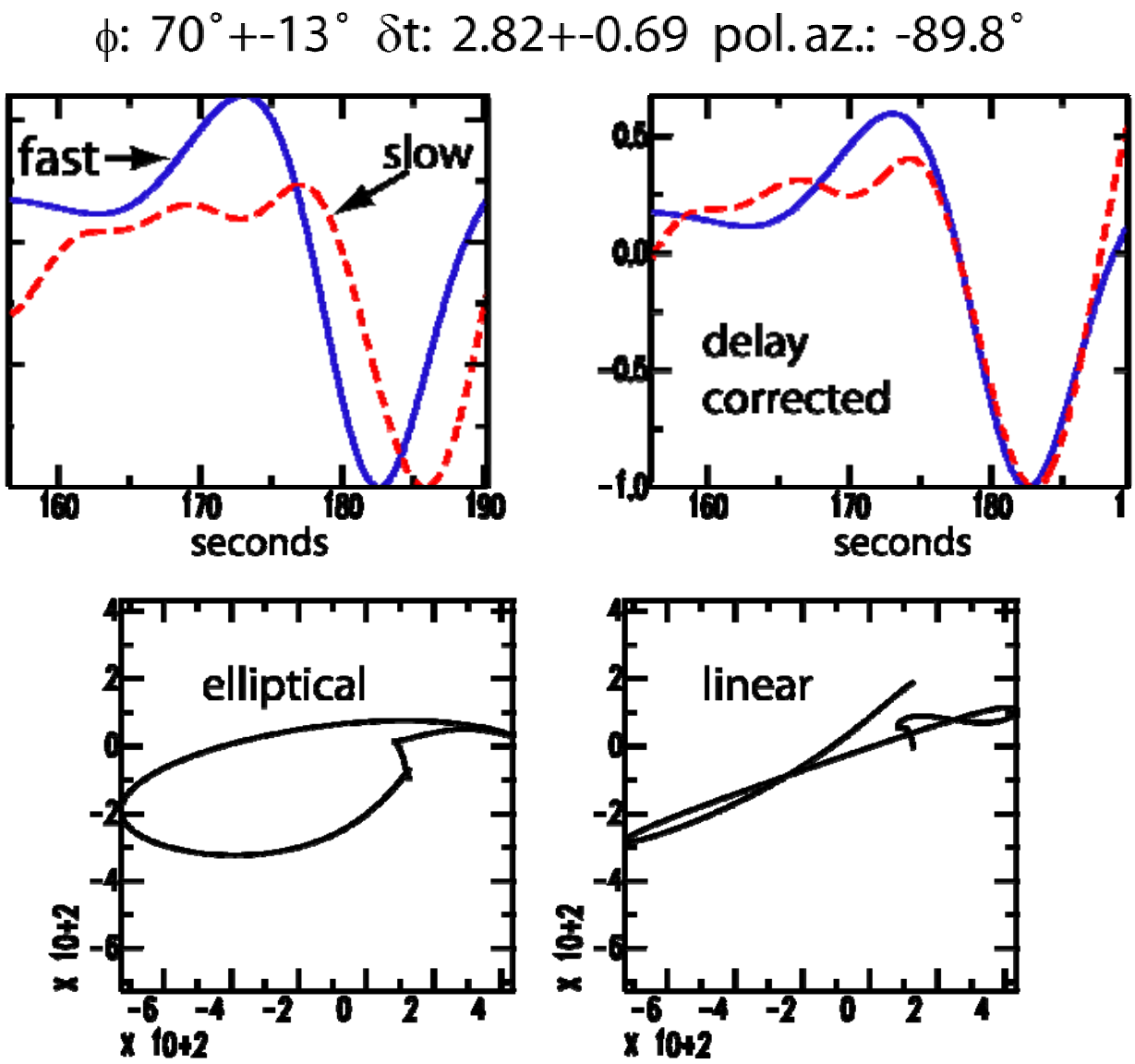

Supp. Figure DR3B. *Particle motion plots for the event shown in Fig. DR3A. Top two traces show the waveform similarity and time separation (left) and the good correspondence between the fast and slow split waves once the delay is corrected (right). Bottom two panels show the elliptical particle motion characteristic of shear wave splitting (left), and the linearized particle motion after splitting correction (right).*

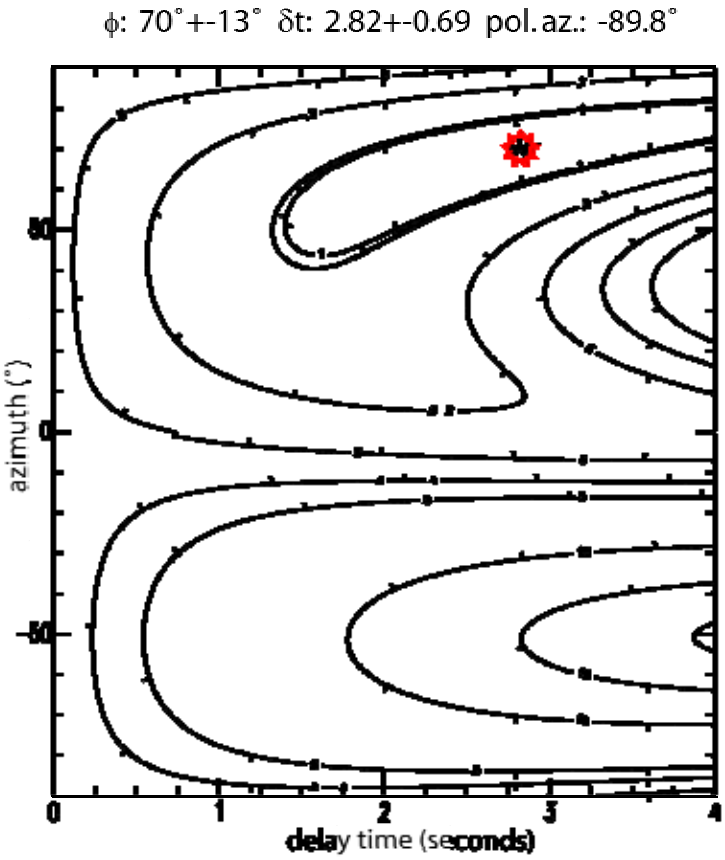

Supp. Figure DR3C. *Contour plot of energy on the horizontal component corresponding to the minimum eigenvalue of the polarization matrix for the SW Indian Ridge event shown in Figures DR7A and DR7B. The energy has a clear and distinct single minimum at nearly 4 s delay time and a fast direction of N5°W (red star). Double lined contour marks the 95% confidence limit for the measurement.*

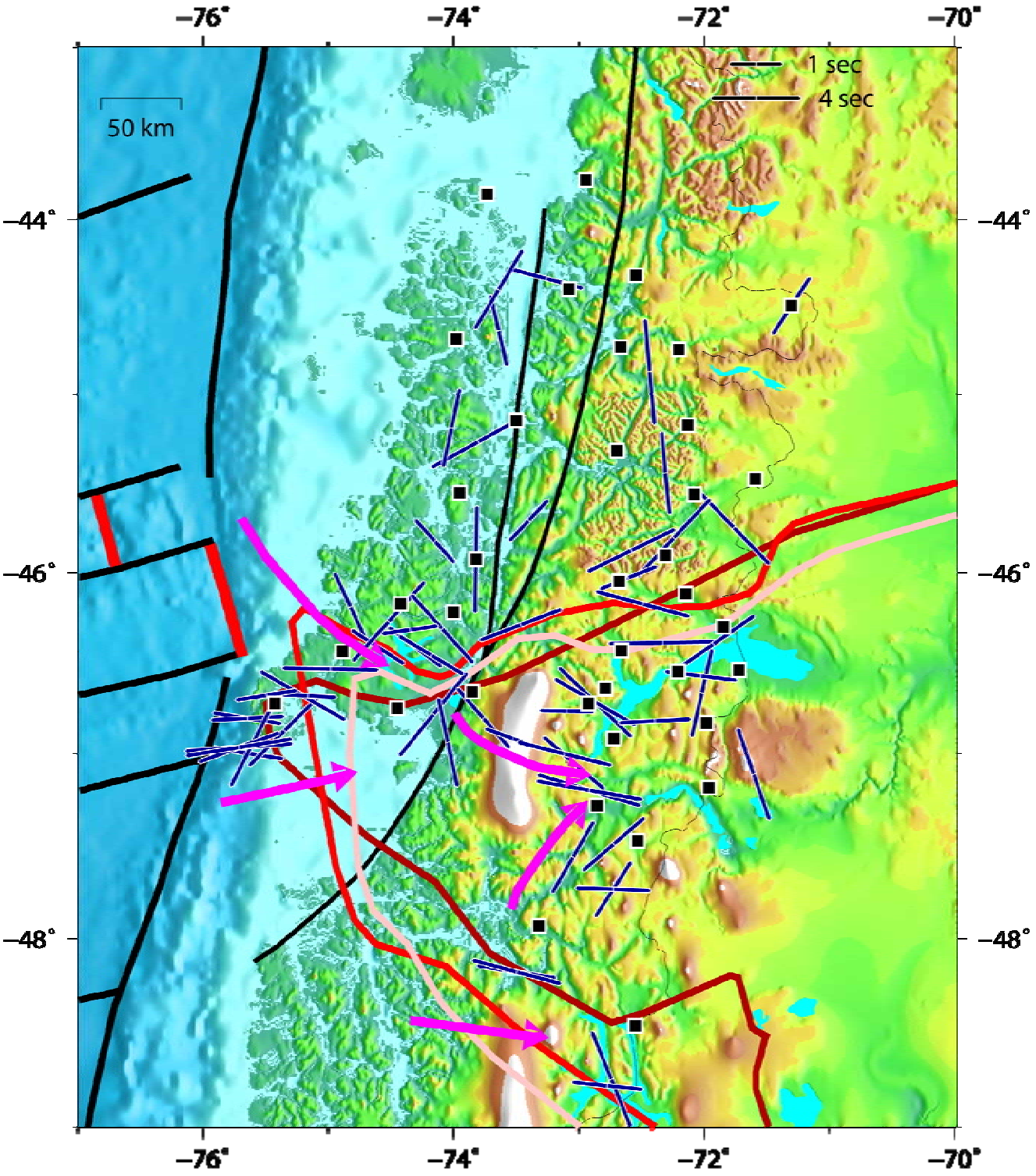

Supp. Fig. DR4*. Shear wave splitting results shown in the main text (Fig. 4), with arrows added to show our interpretation of upper mantle flow fabrics, as delineated by shear wave splitting, in the vicinity of the slab window.*

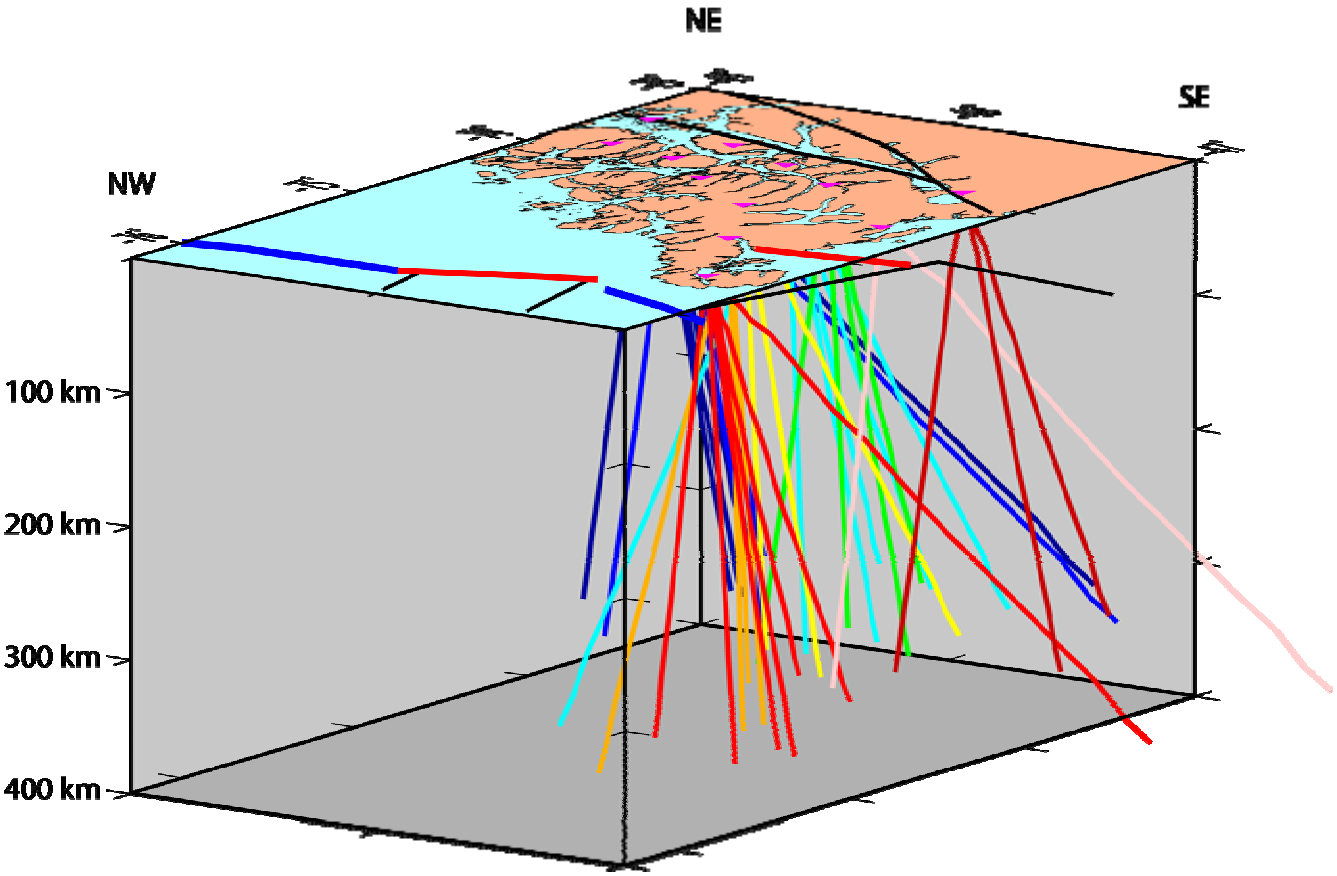

Supp. Fig. DR5. *Ray paths from a quite of up to 7 distinct events arriving at a subset of the CRSP network. Rays to each station color coded; stations shown as purple triangles on block top. Nazca and Antarctic slab structures not shown for clarity. View from the SW toward the NE.*

REFERENCES CITED

Ben Ismail, W., and Mainprice, D., 1998, An olivine fabric database: An overview of upper mantle fabrics and seismic anisotropy: Tectonophys., v. 296, p. 145–157.

Carter, N., Baker, D., and George, R., 1972, Seismic anisotropy, flow and constitution of the upper mantle, *In* Heard, H., I. Borg, N. Carter, C. Raleigh (Eds.), Flow and Fracture of Rocks, Geophys. Mono., v. 16. AGU, Washington, DC, p. 167–190.

Constable, S.C., Parker, R.L., and Constable, C.G., 1987, Occam's inversion: A practical algorithm for generating smooth models from electromagnetic sounding data: Geophysics, v. 52, p. 289–300.

Hess, H.H., 1964, Seismic anisotropy of the uppermost mantle under oceans: Nature, v. 203, p. 629–631.

Huber, P.J., 1981, Robust Statistics, John Wiley & Sons, New York, 320 p.

Jung, H., Katayama, I., Jiang, Z., Hiraga, T., and Karato, S., 2006, Effect of water and stress on the lattice-preferred orientation of olivine: Tectonphys., v. 421, p. 1–22.

Kaminsky, E., and Ribe, N.I., 2001, A kinematic model for recrystallization and texture development in olivine polycrystals: Earth Planet. Sci. Lett., v. 189, p. 253–267.

Mainprice, D. and Silver, P.G., 1993, Interpretation of SKS waves using samples from the subcontinental lithosphere: Phys. Earth Planet. Int., v. 78, p. 257–280.

Neele, F., VanDecar, J.C., and Snieder, R., 1993a, A formalism for including amplitude data in tomographic inversions: Geophys. J. Int., v. 115, p. 482–496.

Neele, F., VanDecar, J.C., and Snieder, R., 1993b, The use of *P*-wave amplitude data in a joint tomographic inversion with travel times for upper-mantle velocity structure: J. Geophys. Res., v. 98, p. 12,033–12,054.

Silver, P.G., and Chan, W.W,. 1991, Shear wave splitting and subcontinental mantle deformation: J. Geophys. Res., v. 96, p. 16,429–16,454.

VanDecar, J.C., and Crosson, R.S., 1990, Determination of teleseismic relative phase arrival times using multi-channel cross-correlation and least squares: Bull. Seism. Soc. Am., v. 80, p. 150–169.

VanDecar, J.C., and Snieder, R., 1994, Obtaining smooth solutions to large, linear, inverse problems: Geophysics, v. 59, p. 818–829.

VanDecar, J.C., James, D.E., and Assumpcao, M., 1995, Seismic evidence for a fossil mantle plume beneath South America and implications for plate driving forces: Nature, v. 378, p. 25–31.

VanDecar, J.C., Russo, R.M., James, D.E., Ambeh, W.B., and Franke, M., 2003, Aseismic Continuation of the Lesser Antilles Slab Beneath Continental South America: J. Geophys. Res., v. 108, 2043, doi:10.1029/2001JB000884.